Ocean Engineering 106 (2015) 472–484

Contents lists available at ScienceDirect

Ocean Engineering

journal homepage: www.elsevier.com/locate/oceaneng

Advanced control for fault-tolerant dynamic positioning of an offshore supply vessel

Flavia Benetazzo, Gianluca Ippoliti *, Sauro Longhi, Paolo Raspa

Dipartimento di Ingegneria dell'Informazione, Universitá Politecnica delle Marche, via brecce bianche 12, 60131 Ancona, Italy

ARTICLE INFO

Article history:
Received 8 May 2014
Accepted 5 July 2015
Available online 4 August 2015

Keywords:
Dynamic positioning
Ship control
Filtering techniques
Sliding mode control
Fault diagnosis
Fault-tolerant systems

ABSTRACT

The paper presents a solution to guarantee a fault-tolerant robust control for the dynamic positioning of an over-actuated offshore supply vessel. Fault detection is obtained by a combination of two model-based techniques: the parity space approach and the Luenberger observer. The dynamic positioning system is provided by a bank of reconfigurable Discrete-Time Variable-Structure Controllers (DTVSC), selected by a supervisor, based on a fault isolation logic. The control system is combined with a wave compensation based on a Multi-rate Extended Kalman Filter (MREKF). The proposed solution is compared with a standard Proportional-Integral-Derivative (PID) control system and a passive nonlinear wave filter to assess its robustness to input disturbances and uncertainties in the model parameters. The simulation tests developed for a scale model of an offshore supply vessel show that, in the case of actuators faults, dynamic positioning is guaranteed by the proposed solution.

1. Introduction

Offshore exploration and exploitation of hydrocarbons have opened up an era of dynamically positioned vessels. Dynamic positioning (DP) is an autonomous control system that acts to maintain vessel position and the angle of direction at a reference point by means of the vessel propulsion and maneuvering thrusters. To calculate the steering angle and the thrust of each thruster, information from sensors (GPS, gyroscopes, etc.) and from the thruster allocation algorithm is combined. The control action maintains the desired position and orientation according to a navigation path or a specific task (absolute or relative DP). The dynamic positioning system is decisive in those situations in which the position of the unit is either bound to a specific point on the seabed (absolute DP), or is related to a moving unit, such as when the ship is operating with other vessels or with remotely operated underwater vehicles. A dynamically positioned vessel is defined by the International Maritime Organization (IMO) and the certifying class societies (DNV, ABS, LR, etc.) as a vessel that maintains its position and heading (fixed location or pre-determined track) exclusively by means of active thrusters (Sørensen, 2011; Johansen et al., 2014). Other solutions, like position mooring, consider the aid of mooring lines, as described by Nguyen and Sørensen (2009), Fang et al. (2015), and Chen et al. (2013). The evaluation of structural responses is key element in the design of ships and offshore structures and Hirdaris et al. (2014) review some of the recent advances in the assessment of loads for ships and offshore structures.

To date most dynamic positioning systems have been used for positioning drill ships in deep water, and for other offshore operations, such as diving support and anchor handling. Furthermore, DP systems have been applied increasingly to shuttle tankers during offloading operations using a floating production, storage and offloading unit (see Sørensen, 2011; Fossen, 2011). The first DP systems were designed using conventional PID controllers in a cascade with low pass and/or notch filters to suppress the wave induced motion components. From 1980 onwards, a new model-based control concept, which exploits stochastic optimal control theory and Kalman filtering techniques, has been employed to address the DP problem (Balchen et al., 1980). Subsequent extensions and modifications of the latter work have been proposed by numerous authors, including Sørensen (2011), Fossen (2000), Strand and Fossen (1999), Fang et al. (2011) and references therein. In Xia et al. (2005) and in Tannuri and Agostinho (2010) the sliding mode control is used with a Passive Nonlinear Observer for the DP problem. A procedure for attenuating the control law of a vessel dynamic positioning system, based on the observer backstepping methodology, is proposed in Morishita and Souza (2014) and a port-Hamiltonian framework to design a nonlinear set-point-regulation controller with integral action is presented in Donaire and Perez (2012). A family of passivity-based controllers for dynamic positioning of ships is considered in Muhammad and Dòria-Cerezo (2012).

* Corresponding author. Tel.: +39 071 220 4382; fax: +39 071 220 4224.
E-mail addresses: f.benetazzo@univpm.it (F. Benetazzo), gianluca.ippoliti@univpm.it (G. Ippoliti), sauro.longhi@univpm.it (S. Longhi), p.raspa@univpm.it (P. Raspa).

http://dx.doi.org/10.1016/j.oceaneng.2015.07.001
0029-8018/

As with other technological systems, a DP system is subject to fault (e.g. loss of position) which may be caused by computer, electrical, hydraulic or thruster failures. The International Marine Contractors Association (IMCA) has defined guidelines for fault-tolerant system design (MSC/IMCA, 1994): a requirement for a DP Class 2 vessel is that loss of position is not to occur in the event of a single failure in any active component or system (generators, thrusters, switchboards, remote controlled valves, etc.). However thrusters cause 21% of the incidents related to DP, according to the report in IMCA (1994), and thruster reliability for DP has been addressed by Phillips (1996) as a problem to be solved. It is very important to recover control authority in case of any thruster failure and the IMCA guidelines for vessels equipped with dynamic positioning systems, MSC/IMCA (1994) require the redundancy of all active components, thrusters included, to meet the single failure criteria given above. Redundancy, as an alternative means of providing the same function, is intended as fault tolerance, which is the ability of a system to continue operating following a failure, and is more general than having at least two of each thruster component.

Single point thruster failures in DP applications are extensively described in Phillips (1998) and early diagnosis and fault-tolerant control for safe operation of floating platforms where mooring systems maintain vessel position and must withstand environmental loads are considered in Fang et al. (2015). Systematic fault-tolerant control was studied for the station keeping of a marine vessel by Blanke (2005) and a structure-graph approach for fault diagnosis and control reconfiguration was validated by sea tests. Fault-tolerant approaches to handle thrust failures have recently been proposed in Fu et al. (2010, 2011): classical PID controls are used and reconfiguration after faults is implemented by means of the virtual actuator approach in Blanke et al. (2006). With this approach the PID controllers may not be sufficiently robust to handle reconfiguration transients during non-steady state maneuvering.

This paper presents an innovative solution for the DP control system of a vessel, based on a bank of reconfigurable Discrete-Time Variable Structure Control (DTVSC) systems selected by a logic supervisor and wave filtering using a Multi-rate Extended Kalman Filter. The introduction of DTVSC allows the issue of control law digitalization to be taken into account directly and it ensures robustness with respect to model uncertainties and input disturbances acting on the actuators. An Extended Kalman Filter (EKF) is designed for the purpose of estimating the disturbances induced by the first order wave forces on the thruster. This is done to minimize the thruster efforts. The estimation is improved by means of a Multi-rate Extended Kalman Filter (MREKF) which allows differences in the working frequency of the sensors to be considered (Wang et al., 2013, 2014). A fault diagnosis module and a control reconfiguration structure are used to handle thruster failures. The proposed solution is compared to a standard PID control system tuned using an LQR algorithm (Fossen, 2011) equipped with a Passive Nonlinear Observer to filter waves (Strand and Fossen, 1999). Tests are based on numerical results.

The paper is organized as follows. The kinematic and dynamic vessel equations, the thruster allocation and the wave model are presented in Section 2. The filter techniques are discussed in Section 3. The fault diagnosis system is presented in Section 4. The control system is reported in Section 5. Simulation results are presented in Section 6. The paper ends with conclusions and comments.

2. Mathematical model of the DP vessel

Motion superposition is the most commonly adopted model for ship motion control system design (Perez and Fossen, 2004). Motion can be conceptually decomposed as the superposition of three contributions:

- slowly varying disturbance motion produced by second order wave effects, current and wind;
- control-induced motion described by a maneuvering model, clarifying the relationship between control action and its effects on the motion. These dynamics are referred to as Low Frequency (LF) dynamics;
- wave-induced motion where the wave frequency oscillatory motion induced by first order waves is described by a sea-keeping model. These dynamics are referred to as Wave Frequency (WF) dynamics.

2.1. Maneuvering model

The generalized displacement and body-fixed velocities are defined as $\boldsymbol{\eta}$ and $\boldsymbol{\nu}$, respectively, where $\boldsymbol{\nu}$ is defined in the ship body-fixed frame $\{b\}$, while $\boldsymbol{\eta}$ is defined in the local geographical inertial north-east-down frame $\{n\}$, fixed to the Earth (Fossen, 2011). The kinematics equations, which express the relationship between the generalized displacements in the $\{n\}$ frame and the velocities in the $\{b\}$ frame, are

$$\dot{\boldsymbol{\eta}} = \boldsymbol{J}(\boldsymbol{\eta})\boldsymbol{\nu} \tag{1}$$

where $\boldsymbol{J}$ is the transformation matrix from the $\{b\}$ to the $\{n\}$ frame.

In case of irrotational and constant ocean currents (Fossen, 2011), the 6 degrees of freedom (DOF) maneuvering equations of motions can be expressed in the $\{b\}$ frame as

$$\boldsymbol{M}\dot{\boldsymbol{\nu}}_r + \boldsymbol{C}(\boldsymbol{\nu}_r)\boldsymbol{\nu}_r + \boldsymbol{D}(\boldsymbol{\nu}_r)\boldsymbol{\nu}_r + \boldsymbol{G}\boldsymbol{\eta} = \boldsymbol{\tau}_c + \boldsymbol{\tau}_{env} \tag{2}$$

where $\boldsymbol{\nu}_r = [u-u_c, v-v_c, w, p, q, r]^T$ is the relative velocity vector between the vessel and the current (see Section 2.2.3); $\boldsymbol{M} = (\boldsymbol{M}_{RB} + \boldsymbol{M}_A)$ is the system inertia matrix, including the rigid-body and the added mass matrices; $\boldsymbol{C} = \boldsymbol{C}_{RB} + \boldsymbol{C}_A(\nu_r)$ is the Coriolis–centripetal matrix, including both rigid-body ($\boldsymbol{C}_{RB}$) and added mass $\boldsymbol{C}_A(\nu_r)$; $\boldsymbol{D}(\nu_r) = \boldsymbol{D}_L + \boldsymbol{D}_{NL}(\nu_r, \gamma_r)$ is the damping matrix, which may be divided into a linear component ($\boldsymbol{D}_L$), accounting for linear wave drift damping and laminar skin frictions and a non-linear component ($\boldsymbol{D}_{NL}(\nu_r, \gamma_r)$) accounting for the effects of ocean currents. It is important to notice that, for velocities of vessel close to zero, the linear damping becomes more significant than the nonlinear damping. The restoring term is assumed to be $\boldsymbol{G}(\eta) = \boldsymbol{G}\eta$ under the assumption of small roll and pitch angles. The terms $\boldsymbol{\tau}_c$ are the control forces and moments to be produced by the actuators, while $\boldsymbol{\tau}_{env}$ are the environmental loads.

2.2. Environmental forces and moments

A ship in a seaway is mainly affected by the following types of environmental disturbances: waves, currents, and wind. The environmental disturbances contain both slowly varying and high-frequency forces. Control forces and moments due to environmental disturbances are caused by wind and waves. Using the principle of superposition, they are added to the right side of (2) by defining $\boldsymbol{\tau}_{env} = \boldsymbol{\tau}_{wind} + \boldsymbol{\tau}_{wave}$.

2.2.1. Wind forces and moments

The wind force on a marine vessel is proportional to the projected area above the waterline and to the square of the wind speed relative to the vessel. The total relative wind speed can be defined as

$$U_{rw} = \sqrt{u_{rw}^2 + v_{rw}^2} \tag{3}$$

where $u_w = u - V_w \cos(\gamma_{rw})$ and $v_w = v - V_w \sin(\gamma_{rw})$ are the wind speeds components, V_w is the wind velocity, $\gamma_{rw} = \beta_w - \psi$ is the relative wind angle and β_w is the wind direction. The above parameters are expressed in the $\{n\}$ frame (see Fig. 1). The wind loads are given by (Fossen, 2011)

$$\boldsymbol{\tau}_{wind} = \frac{1}{2}\rho_a U_{rw}|U_{rw}| \begin{bmatrix} C_X(\gamma_{rw})A_{F_w} \\ C_Y(\gamma_{rw})A_{L_w} \\ C_Z(\gamma_{rw})A_{F_w} \\ C_K(\gamma_{rw})A_{L_w}H_{L_w} \\ C_M(\gamma_{rw})A_{F_w}H_{F_w} \\ C_N(\gamma_{rw})A_{L_w}L_{oa} \end{bmatrix} \tag{4}$$

where ρ_a is the air density; H_{F_w} and H_{L_w} are the centroids above the water line of the frontal (A_{F_w}) and lateral (A_{L_w}) projected areas of the non-submerged part of the ship projected on the *xz*- and the *yz*-plane, respectively; L_{oa} is the overall length of vessel and the terms C_X, C_Y, C_Z, C_K, C_M, C_N are non-dimensional wind coefficients derived by model testing or by semi-empirical formulas, as in Isherwood (1972).

2.2.2. Wave forces and moments

When designing a DP control system it is important to evaluate the robustness and performance in the presence of waves. A motion control system can be simulated under influence of wave-induced forces by separating two effects: the 1st order wave-induced forces, τ_{wave1}, wave loads observed as zero-mean oscillatory components and the 2nd order wave-induced forces, τ_{wave2}, wave drifts forces observed as non-zero slowly varying components. According to Fossen (2011) wave forces can be modeled by a linear superposition of the two components, therefore $\tau_{wave} = \tau_{wave1} + \tau_{wave2}$.

Wave force models depend on response amplitude operators (RAOs) computed for the particular craft using a hydrodynamic program from hull geometry. For each degree of freedom (DOF $\in \{1 \ldots 6\}$) in (2), the wave loads and drifts can be represented as a sum of a large number N of sinusoidal components:

$$\tau_{wave1}^{\{\mathrm{DOF}\}} = \sum_{k=1}^{N} \rho_w g \left| F_{wave1}^{\{DOF\}} \right| A_k \cos\left(\omega_{e_k} t + \angle F_{wave1}^{\{DOF\}} + \epsilon_k\right)$$

$$\tau_{wave2}^{\{\mathrm{DOF}\}} = \sum_{k=1}^{N} \rho_w g \left| F_{wave2}^{\{DOF\}} \right| A_k^2 \cos\left(\omega_{e_k} t + \epsilon_k\right) \tag{5}$$

where the normalized force RAO $F_{wavei}^{\{\mathrm{DOF}\}} = F_{wavei}^{\{\mathrm{DOF}\}}(\omega_k, \beta_{wave})$, $i = 1, 2$, are complex variables depending on the wave frequency component

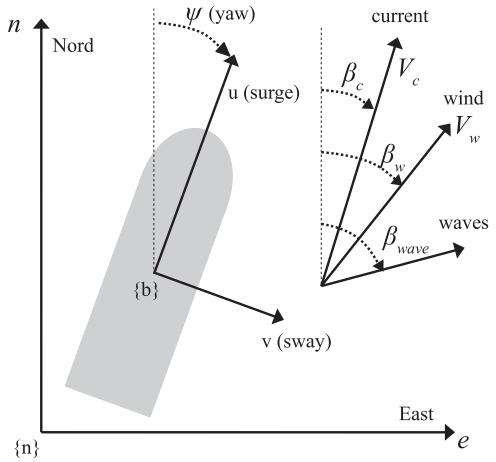

Fig. 1. Reference frames definition: $\{n\}$ and $\{b\}$ frames, waves, current and wind directions.

ω_k and the relative wave direction β_{wave}, ρ_w is the water density, A_k is the wave amplitude for the wave component k, depending on the wave spectrum, significant wave height H_s and modal frequency w_0. The wave encounter frequency is $\omega_{e_k} = \omega_k - (\omega_k^2 U \cos(\beta_{wave}))/(2g)$, where U is the ship forward velocity and ϵ_k is a random phase component drawn from a uniform distribution in $[-\pi\ \pi]$, to ensure stationarity of the time series.

2.2.3. Ocean current forces and moments

The effect of sea current can be divided into two components: potential and viscous. The potential component of current includes the Munk moment and is formulated according to Sørensen et al. (1996) as $\boldsymbol{C_A}(\nu_r)$ in (2). The horizontal current components in surge and sway are defined as

$$u_c = V_c \cos(\beta_c - \psi), \quad v_c = V_c \sin(\beta_c - \psi), \tag{6}$$

where V_c and β_c are the current velocity and direction, respectively, see Fig. 1. The total relative current vector is then defined as

$$U_{cr} = \sqrt{u_r^2 + v_r^2}, \tag{7}$$

where $u_r = u - u_c$, and $v_r = v - v_c$. The effect of the current is normally included in the nonlinear damping term $D_{NL}(\nu_r, \gamma_r)$ of (2) as a function of the relative velocity vector ν_r and the relative drag angle, $\gamma_r = \arctan(-v_r, u_r)$.

2.3. Motion control model

The motion of a surface vessel for the development of a dynamic positioning control system is described by a model which is based on the common assumption that only slow horizontal motion must be counteracted, as stated in Fossen (2011). In this hypothesis the generalized velocity vector $\boldsymbol{\nu} \triangleq [u, v, r]^T$ in the $\{b\}$ frame is considered, where u is the surge velocity, v is the sway velocity and r is the yaw rate (see Fig. 1). The ship position is referred to the $\{n\}$ frame and described by the generalized position $\boldsymbol{\eta} \triangleq [n, e, \psi]^T$, where n and e are the ship position in the $\{n\}$ frame and ψ is the ship orientation referred to the n frame. Under the assumption of low-speed maneuvering the quadratic terms of velocity, the Coriolis terms and the nonlinear damping terms are neglected. With the above-mentioned notation, the 3 DOF DP model used to develop the control system is described by the following dynamics:

$$\boldsymbol{M}\dot{\boldsymbol{\nu}}_{LF} + \boldsymbol{D}\boldsymbol{\nu}_{LF} = \boldsymbol{\tau}_c + \boldsymbol{\tau}_{env}, \tag{8}$$

where $\boldsymbol{\nu}_{LF}$ is the low-frequency generalized velocity vector. The kinematic equation has the following form:

$$\dot{\boldsymbol{\eta}}_{LF} = \boldsymbol{R}(\psi)\boldsymbol{\nu}_{LF}, \tag{9}$$

where the matrix $\boldsymbol{R}(\psi)$ describes rotation from $\{b\}$ frame to $\{n\}$ frame:

$$\boldsymbol{R}(\psi) = \begin{bmatrix} \cos\psi & -\sin\psi & 0 \\ \sin\psi & \cos\psi & 0 \\ 0 & 0 & 1 \end{bmatrix}. \tag{10}$$

2.3.1. Environmental disturbances

In the considered motion control model, environmental disturbances include both slowly varying and high frequency forces and moments. The slowly varying disturbances include second order wave drift, ocean currents and wind forces. These effects are modeled, as in Fossen (2011), by a bias $\boldsymbol{b}$, described by the following dynamic equation:

$$\dot{\boldsymbol{b}} = \boldsymbol{w}_b, \tag{11}$$

where $\boldsymbol{w}_b \sim \mathcal{N}(0, \boldsymbol{Q}_b)$ is a white noise with zero mean and covariance matrix $\boldsymbol{Q}_b$. This environmental disturbance force, referred to the ship body frame $\{b\}$, has the form

$$\boldsymbol{\tau}_{env} = \boldsymbol{R}(\psi)^T \boldsymbol{b}.$$

First order wave force effects on ship motion on the 3DOF are modeled in the Wave Frequency (WF) dynamics by three second order systems of which the state-space form is

$$\underbrace{\begin{bmatrix}\dot{\xi}_1\\ \dot{\xi}_2\\ \dot{\xi}_3\\ \dot{\xi}_4\\ \dot{\xi}_5\\ \dot{\xi}_6\end{bmatrix}}_{\dot{\boldsymbol{\xi}}} = \underbrace{\begin{bmatrix} 0 & 1 & 0 & 0 & 0 & 0\\ -\omega_{0_n}^2 & -2\lambda_{w_n}\omega_{0_n} & 0 & 0 & 0 & 0\\ 0 & 0 & 0 & 1 & 0 & 0\\ 0 & 0 & -\omega_{0_e}^2 & -2\lambda_{w_e}\omega_{0_e} & 0 & 0\\ 0 & 0 & 0 & 0 & 0 & 1\\ 0 & 0 & 0 & 0 & -\omega_{0_\psi}^2 & -2\lambda_{w_\psi}\omega_{0_\psi}\end{bmatrix}}_{\boldsymbol{A}_w} \underbrace{\begin{bmatrix}\xi_1\\ \xi_2\\ \xi_3\\ \xi_4\\ \xi_5\\ \xi_6\end{bmatrix}}_{\boldsymbol{\xi}}$$

$$+ \underbrace{\begin{bmatrix} 0 & 0 & 0\\ K_{w_n} & 0 & 0\\ 0 & 0 & 0\\ 0 & K_{w_e} & 0\\ 0 & 0 & 0\\ 0 & 0 & K_{w_\psi}\end{bmatrix}}_{\boldsymbol{E}_w} \boldsymbol{w}_w; \boldsymbol{\eta}_{WF} = \underbrace{\begin{bmatrix} 0 & 1 & 0 & 0 & 0 & 0\\ 0 & 0 & 0 & 1 & 0 & 0\\ 0 & 0 & 0 & 0 & 0 & 1\end{bmatrix}}_{\boldsymbol{C}_w} \begin{bmatrix}\xi_1\\ \xi_2\\ \xi_3\\ \xi_4\\ \xi_5\\ \xi_6\end{bmatrix} \tag{12}$$

where the components of the position vector $\boldsymbol{\eta}_{WF}$ are the responses of three linear ship wave models in surge, sway and yaw, the terms $K_{w_i} = 2\lambda_{w_i}\omega_{0_i}\sigma_{w_i}$ with $i \in \{n, e, \psi\}$ represent constant gains, where σ_{w_i} is a constant describing the wave intensity (Fossen, 2011), λ_{w_i} are damping coefficients and ω_{0_i} is the dominating wave frequency for $i \in \{n, e, \psi\}$, and $\boldsymbol{w}_w = [w_{w_n}, w_{w_e}, w_{w_\psi}]^T \sim \mathcal{N}(0, \boldsymbol{Q}_w)$ is a white noise with zero mean and covariance matrix $\boldsymbol{Q}_w$ (Fossen, 2011). These parameters are estimated using the technique described in Fossen and Perez (2009) when there are significant changes in heading and at regular intervals of 1200 s, which is the time period for which the sea state can be considered stationary.

2.3.2. Thruster allocation

Marine vessels with n DOF are characterized by n generalized control forces $\boldsymbol{\tau}_c \in \Re^n$ which are distributed among the r thrusters in terms of control inputs $\boldsymbol{u} \in \Re^r$:

$$\boldsymbol{\tau}_c = \boldsymbol{T}(\boldsymbol{\alpha})\boldsymbol{u} \tag{13}$$

where $\boldsymbol{u}$ is the thrust force vector. The thruster configuration matrix $\boldsymbol{T}(\boldsymbol{\alpha})$ depends on the location and orientation of the thrusters. The considered 3DOF offshore supply vessel has two main propellers, two tunnel thrusters and two azimuth thrusters, as shown in Fig. 2 and described in Table 1. The azimuth thruster headings are maintained at fixed angles $\overline{\alpha}_5$ and $\overline{\alpha}_6$. For the considered vessel the thruster configuration matrix $\overline{\boldsymbol{T}}$ has the form

$$\overline{\boldsymbol{T}} = \boldsymbol{T}(\overline{\boldsymbol{\alpha}}) = \begin{bmatrix} 1 & 1 & 0 & 0 & \cos\overline{\alpha}_5 & \cos\overline{\alpha}_6\\ 0 & 0 & 1 & 1 & \sin\overline{\alpha}_5 & \sin\overline{\alpha}_6\\ -l_1 & l_2 & l_3 & -l_4 & l_5\sin\overline{\alpha}_5 & -l_6\sin\overline{\alpha}_6\end{bmatrix}. \tag{14}$$

Referring to the thruster configuration matrix in (14), Fig. 2 shows that the allocation of the 6 thrusters is symmetrical with respect to the longitudinal axis of the vessel. Considering the two main propellers, the two tunnel thrusters and the two azimuth thrusters as three pair of symmetrical thrusters, the same torque demand is applied to both the thrusters in each pair when there are no faults and disturbances on the actuators. Therefore the following condition is assumed:

$$u_i = u_{i+1} \quad \text{for} \quad i = 1, 3, 5. \tag{15}$$

The thruster failures are modeled as additive faults, because a loss of torque for a thruster is modeled using an equal torque for the corresponding element of the $\boldsymbol{f}$ torque vector. In the same way, the input disturbances $\boldsymbol{d}$ are modeled as slowly varying biases, described by the dynamics equation $\dot{\boldsymbol{d}} = \boldsymbol{w}_d$, where $\boldsymbol{w}_d \sim \mathcal{N}(\boldsymbol{0}, \boldsymbol{Q}_d)$ is a white noise source. Therefore the inclusion of faults and input disturbances transforms the thruster allocation as follows:

$$\boldsymbol{\tau}_c = \overline{\boldsymbol{T}}(\boldsymbol{u} + \boldsymbol{d} + \boldsymbol{f}). \tag{16}$$

2.3.3. Dynamic positioning model

Under the above considered hypothesis the dynamic positioning model has the following form:

$$\begin{aligned}&\dot{\boldsymbol{\xi}} = \boldsymbol{A}_w\boldsymbol{\xi} + \boldsymbol{E}_w\boldsymbol{w}_w, \dot{\boldsymbol{\eta}}_{\mathrm{LF}} = \boldsymbol{R}(\psi)\boldsymbol{\nu}_{\mathrm{LF}}, \dot{\boldsymbol{b}} = \boldsymbol{w}_b, \dot{\boldsymbol{d}} = \boldsymbol{w}_d,\\ &\boldsymbol{M}\dot{\boldsymbol{\nu}}_{\mathrm{LF}} = -\boldsymbol{D}\boldsymbol{\nu}_{\mathrm{LF}} + \overline{\boldsymbol{T}}(\boldsymbol{u} + \boldsymbol{d} + \boldsymbol{f}) - \boldsymbol{R}(\psi)^T\boldsymbol{b} + \boldsymbol{w}_{\nu_{\mathrm{LF}}}, \boldsymbol{\eta}_m = \boldsymbol{\eta}_{\mathrm{LF}} + \boldsymbol{C}_w\boldsymbol{\xi} + \boldsymbol{w}_\eta.\end{aligned} \tag{17}$$

where $\boldsymbol{w}_{\nu_{LF}} \sim \mathcal{N}(\boldsymbol{0}, \boldsymbol{Q}_\nu)$ is a white noise process representing the model inaccuracies. Defining the state vector $\boldsymbol{x} = [\boldsymbol{\xi}^T, \boldsymbol{\eta}_{LF}^T, \boldsymbol{b}^T, \boldsymbol{d}^T, \boldsymbol{\nu}_{LF}^T]^T \in \Re^{21}$ and the measured ship position $\boldsymbol{\eta}_m \in \Re^3$ in the $\{n\}$ frame as the superposition of LF and WF dynamics, the DP model in (17) has the following nonlinear state-space form:

$$\begin{aligned}\dot{\boldsymbol{x}} = &\underbrace{\begin{bmatrix}\boldsymbol{A}_w & 0 & 0 & 0 & 0\\ 0 & 0 & 0 & 0 & \boldsymbol{R}(\psi)\\ 0 & 0 & 0 & 0 & 0\\ 0 & 0 & 0 & 0 & 0\\ 0 & 0 & -\boldsymbol{M}^{-1}\boldsymbol{R}(\psi)^T & \boldsymbol{M}^{-1}\overline{\boldsymbol{T}} & -\boldsymbol{M}^{-1}\boldsymbol{D}\end{bmatrix}}_{\boldsymbol{f}(\boldsymbol{x})}\boldsymbol{x}\\ &+ \underbrace{\begin{bmatrix}0\\ 0\\ 0\\ 0\\ \boldsymbol{M}^{-1}\overline{\boldsymbol{T}}\end{bmatrix}}_{\boldsymbol{B}}(\boldsymbol{u} + \boldsymbol{d} + \boldsymbol{f}) + \underbrace{\begin{bmatrix}\boldsymbol{E}_w & 0 & 0 & 0\\ 0 & 0 & 0 & 0\\ 0 & \boldsymbol{I} & 0 & 0\\ 0 & 0 & \boldsymbol{I} & 0\\ 0 & 0 & 0 & \boldsymbol{M}^{-1}\end{bmatrix}}_{\boldsymbol{E}}\boldsymbol{w}, \boldsymbol{\eta}_m\\ = &\underbrace{[\boldsymbol{C}_w\ \boldsymbol{I}\ 0\ 0\ 0]}_{\boldsymbol{H}}\boldsymbol{x} + \boldsymbol{w}_\eta,\end{aligned} \tag{18}$$

where $\boldsymbol{w} = [\boldsymbol{w}_w^T, \boldsymbol{w}_b^T, \boldsymbol{w}_d^T, \boldsymbol{w}_\nu^T]^T$ is the state white noise vector with covariance $\boldsymbol{Q} = \mathrm{diag}\{\boldsymbol{Q}_w, \boldsymbol{Q}_b, \boldsymbol{Q}_d, \boldsymbol{Q}_\nu\}$, $\boldsymbol{f}(\boldsymbol{x})$ is the nonlinear state transition term, $\boldsymbol{B}$ is the control input matrix and $\boldsymbol{E}$ is the state disturbance matrix, $\boldsymbol{H}$ is the output transition matrix and $\boldsymbol{w}_\eta \sim \mathcal{N}(\boldsymbol{0}, \boldsymbol{Q}_\eta)$ is the white noise process modeling the measurement error.

3. Wave filtering

To reduce wear and tear on both the steering machine and thrusters modulation, commercial autopilot and DP systems have some kind of wave filtering (Fossen, 2011; Perera et al., 2012). A wave filter is usually a model-based observer which separates the position and heading measurements into a Low-Frequency (LF) and Wave-Frequency (WF) position and heading part. It is important that only the slowly varying disturbances are counteracted by the steering and propulsion systems; the oscillatory motion due to the waves (1st-order wave-induced disturbances) should be prevented from entering the control feedback loop in order to avoid unnecessary usage of the actuators (thrust modulation) (Fossen, 2011). In particular, in this paper a Discrete-time Extended Kalman Filter (Benetazzo et al., 2012), based on the model (18), is considered to reconstruct the LF motion component from noisy measurements. Assuming the control input $\boldsymbol{u}(t) = \boldsymbol{u}(k)$ for $t \in [kT_s, (k+1)T_s]$, where T_s is the sampling time, the model (18) is linearized around the current state prediction estimate $\hat{\boldsymbol{x}}_{k+1/k}$ to

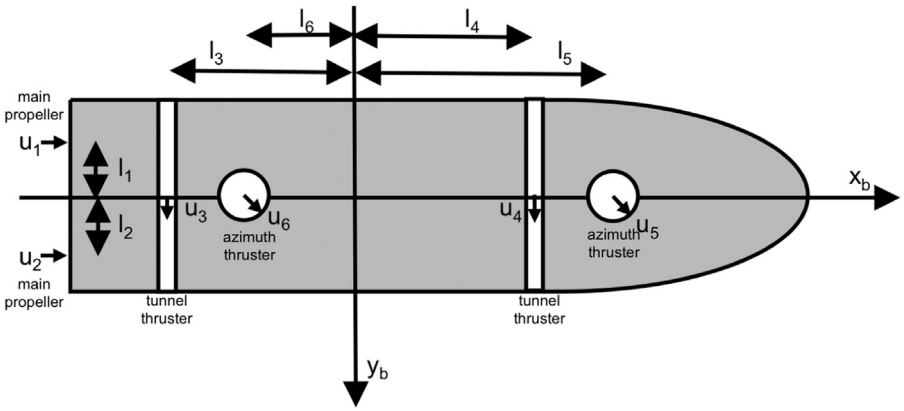

Fig. 2. Thruster configuration for the offshore supply vessel.

Table 1
Thruster configuration matrix.

Thruster	Torque	Angle
Port main propeller	u_1	0
Starboard main propeller	u_2	0
Bow tunnel thruster	u_3	$\pi/2$
Aft tunnel thruster	u_4	$\pi/2$
Bow azimuth thruster	u_5	α_5
Aft azimuth thruster	u_6	α_6

obtain an Extended Kalman Filter with an effective state prediction equation. The terms $\boldsymbol{B}$, $\boldsymbol{E}$ and $\boldsymbol{H}$ are linear, the state matrix $\boldsymbol{f}(x)$ is linearized as

$$\boldsymbol{A}_c = \frac{\partial}{\partial \boldsymbol{x}} \boldsymbol{f}(\boldsymbol{x})|_{\hat{\boldsymbol{x}}_{k+1/k}}. \tag{19}$$

The discretization of this linear model, using a Zero Order Hold (ZOH) with period T_s, produces the linear discrete-time model of the following form (Fossen, 2011):

$$\boldsymbol{x}(k) = \boldsymbol{A}_D \boldsymbol{x}(k-1) + \boldsymbol{B}_D \boldsymbol{u}(k-1) + \boldsymbol{E}_D \boldsymbol{w}(k-1)$$
$$\boldsymbol{y}(k) = \boldsymbol{H}\boldsymbol{x}(k) + \boldsymbol{w}_\eta(k)$$

with

$$\boldsymbol{A}_D = e^{\boldsymbol{A}_c T_s}$$
$$\boldsymbol{B}_D = \left(\int_0^{T_s} e^{\boldsymbol{A}_c \tau}\, \mathrm{d}\tau\right)\boldsymbol{B} = \boldsymbol{A}_c^{-1}(\boldsymbol{A}_D - \boldsymbol{I})\boldsymbol{B}$$
$$\boldsymbol{E}_D = \left(\int_0^{T_s} \mathrm{e}^{\boldsymbol{A}_c \tau}\, \mathrm{d}\tau\right)\boldsymbol{E} = \boldsymbol{A}_c^{-1}(\boldsymbol{A}_D - \boldsymbol{I})\boldsymbol{E}$$
$$\boldsymbol{Q}_D = \int_0^{T_s} \mathrm{e}^{\boldsymbol{A}_c \tau} \boldsymbol{Q} \mathrm{e}^{\boldsymbol{A}_c^T \tau}\, \mathrm{d}\tau = \boldsymbol{Q}T_s + \left(\boldsymbol{A}_c\boldsymbol{Q} + \boldsymbol{Q}\boldsymbol{A}_c^T\right)\frac{T_s^2}{2} + \boldsymbol{A}\boldsymbol{Q}\boldsymbol{A}^T\frac{T_s^3}{3}. \tag{20}$$

The discrete-time EKF has the following form (Jetto et al., 1999):

$$\begin{aligned}
&\boldsymbol{P}_{k+1/k} = \boldsymbol{A}_D \boldsymbol{P}_{k/k} \boldsymbol{A}_D^T + \boldsymbol{Q}_\nu \boldsymbol{E}_D \boldsymbol{Q} \boldsymbol{E}_D^T,\\
&\boldsymbol{K}_{k+1} = \boldsymbol{P}_{k+1/k}\boldsymbol{H}^T(\boldsymbol{H}\boldsymbol{P}_{k+1/k}\boldsymbol{H}^T + \boldsymbol{R})^{-1},\\
&\hat{\boldsymbol{x}}_{k+1/k+1} = \hat{\boldsymbol{x}}_{k+1/k} + \boldsymbol{K}_{k+1}(\boldsymbol{\eta}_m(k) - \boldsymbol{H}\hat{\boldsymbol{x}}_{k+1/k}),\\
&\boldsymbol{P}_{k+1/k+1} = (\boldsymbol{I} - \boldsymbol{K}_{k+1}\boldsymbol{H})\boldsymbol{P}_{k+1/k},\\
&\hat{\boldsymbol{x}}_{k+1/k} = \boldsymbol{\Phi}_{k-1}\hat{\boldsymbol{x}}_{k/k} + \boldsymbol{f}(\hat{\boldsymbol{x}}_{k/k-1}) - \boldsymbol{A}_c\hat{\boldsymbol{x}}_{k/k-1} + \boldsymbol{B}T_s\boldsymbol{u}(k)
\end{aligned} \tag{21}$$

where explicit dependence on T_s has been dropped for simplicity of notation. The term $\boldsymbol{R}$ is the output covariance weight matrix. The implementation of the Kalman filter requires the estimation of the parameter of the model (20). For more details see Fossen (2011) and Fu et al. (2010).

3.1. Multi-rate Kalman Filter

The sensors (GPS and compass) measuring the ship motion $\boldsymbol{\eta}_m$ in (18) do not work at the same frequency and not all measures are available at each sampling instant. The multi-rate model based on the *delta-functions* is considered (Mora and Tornero, 2008). The introduction of the *delta functions* modifies the expression of the Kalman gain indicating the presence or the absence of measurements at each sampling instant, as follows:

$$\boldsymbol{K}_{k+1} = \boldsymbol{P}_{k+1/k}\boldsymbol{H}^T(\boldsymbol{H}\boldsymbol{P}_{k+1/k}\boldsymbol{H}^T + \boldsymbol{R})^{-1} \cdot \boldsymbol{\Delta}_k. \tag{22}$$

The Kalman filter is composed of a prediction and a correction, made through the sensor measurements. In this formulation when measurements are not available, the Multi-rate Kalman Filter only predicts, placing a zero in the $\boldsymbol{\Delta}_k$ matrix (Mora and Tornero, 2008); when new measurements are available the $\boldsymbol{\Delta}_k$ matrix is unitary.

4. Fault diagnosis

4.1. Thruster failures

Phillips (1998) states that regardless of the amount of hardware redundancy installed, all control systems could fail in an instant even if they were thought to be redundant. However, by adopting proper fault-tolerant techniques the chances are greatly reduced. Thruster failure scenarios are listed in Phillips (1998) and DP classification is given according to DP class requirements. In the considered scenario the aim is to meet the requirements of a DP class 2 vessel, i.e. loss of position is not to occur in the event of a single failure in any thruster, and faults are modeled as additive components (see Section 2.3.2).

4.2. Fault diagnosis

The fault diagnosis module proposed in this work is designed to detect failures affecting the thrusters. This module includes the fault analysis module (composed of structural properties and residual generation, that uses two model-based techniques), the fault detection module (using a change detection algorithm) and the logic decision module (used to isolate faults). The fault diagnosis module is used to reconfigure the control input according to the fault-tolerant system architecture shown in Fig. 3.

4.2.1. Structural analysis

It is possible to start investigating the structural properties of a dynamic system by analyzing the structure of the model. The

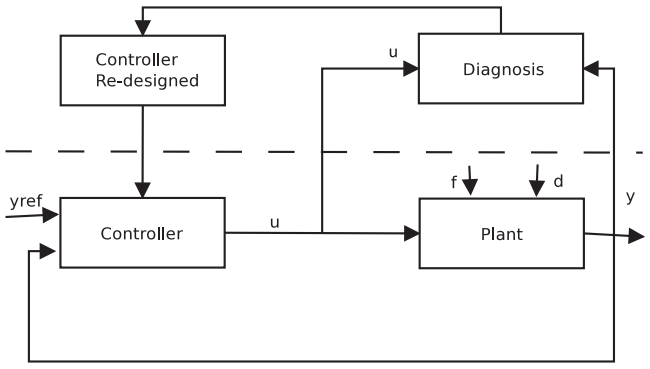

Fig. 3. Fault-tolerant system architecture.

structural model of a system is an abstraction of its behavioral model, in which only the structure of the constraints is considered but not the constraints themselves. As stated in Cocquempot et al. (1998) the structural analysis is the study of the properties which are independent of the actual values of the parameters. Only links between the variables and parameters which result from the operating model are represented in this analysis. They are independent from the operating model and are thus independent of the form under which this operating model is expressed (qualitative or quantitative data, analytical or non-analytical relations). The links are represented by a graph, on which a structural analysis is performed. Considering the maneuvering model of the ship, without considering the environmental disturbances and faults to emphasize the structure of the system, $\boldsymbol{\tau}_c$ from (13), the set of constraints $c_i, i=1,2,3$ for the ship model is classified as below:

$$\begin{aligned}
&\text{algebraic constraints } c_1: \quad \dot{\boldsymbol{\nu}}_{\mathrm{LF}}+\underbrace{\boldsymbol{M}^{-1}\boldsymbol{D}}_{\boldsymbol{\alpha}}\boldsymbol{\nu}_{LF}+\underbrace{\boldsymbol{M}^{-1}}_{\boldsymbol{\beta}}\boldsymbol{\tau}_c=0\\
&\text{differential constraints } c_2: \quad \dot{\boldsymbol{\nu}}_{\mathrm{LF}}-\frac{d}{dt}\boldsymbol{\nu}_{\mathrm{LF}}=0\\
&\text{measurement constraints } c_3: \quad \boldsymbol{\nu}_m-\boldsymbol{\nu}_{\mathrm{LF}}=0
\end{aligned} \tag{23}$$

Normal operation means all functional relations are intact for the system. Should faults occur, one or more functional relations in (23) cease to be valid. The set of known variables is

$$X_{known}=\{\boldsymbol{\tau}_c,\boldsymbol{\nu}_m\} \tag{24}$$

and the set of unknown variables is

$$X_{unknown}=\{\boldsymbol{\nu}_{LF},\dot{\boldsymbol{\nu}}_{LF}\}. \tag{25}$$

Considering the set of variables $\overline{X}=X_{known}\cup X_{unknown}$, the structure is described by the following binary relation:

$$\begin{aligned}
&S: C\times\overline{X}\rightarrow(0,1)\\
&(c_i,\overline{x}_i)\rightarrow\begin{cases}S(c_i,\overline{x}_j)=1 & \text{iff } c_i \text{ applies to } \overline{x}_j,\\ S(c_i,\overline{x}_j)=0 & \text{otherwise.}\end{cases}
\end{aligned} \tag{26}$$

The considered structure can be represented by a table or equivalently by a digraph as there exists a surjective mapping between these two representations. The elimination procedure of the unknown variables $X_{unknown}$ in the functional relations in (23) results in obtaining the parity equations or the so-called Analytical Redundancy Relations (ARR). The procedure is based on the notion of a complete matching in a digraph, as explained in Blanke et al. (2006) and a possible matching is provided implementing the model in the SaTool software, as described in Lorentzen and Blanke (2005), that provides knowledge about the fundamental properties of the system in normal and faulty conditions. Analyzing the link between the variables and the constraints and assuming that only the thrusters can fail, the parity equations that are considered are those regarding the thrusters:

$$\begin{aligned}
&ARR_1: \quad \dot{u}+\alpha_{11}u+\alpha_{13}w+\alpha_{15}q-\beta_{11}\tau_{c_n}=0\\
&ARR_2: \quad \dot{v}+\alpha_{22}v+\alpha_{24}p+\alpha_{26}r-\beta_{22}\tau_{c_e}-\beta_{26}\tau_{c_\psi}=0\\
&ARR_3: \quad \dot{r}+\alpha_{62}v+\alpha_{64}p+\alpha_{66}r-\beta_{62}\tau_{c_e}-\beta_{66}\tau_{c_\psi}=0.
\end{aligned} \tag{27}$$

Relations in (27) give hints on the structural properties of the system, but they cannot be used in actual implementations, because they are derived by a deterministic system and the influence of environmental disturbances can lead to a violation of the ARR in (27) also in faultless conditions, for that reason the parity space approach in Section 4.2.2 is implemented.

The dependability matrix in Table 2 shows the link between parity equations and thrusters and it is used to evaluate the structural properties of the system, showing the relation among ARR in (27) and constraints in (23), grouped in subsystems. Analyzing the dependability matrix of Table 2 the following statements are derived: every violation on each subsystem constraint is detectable, because any fault changing the relations of each subsystems results in a violation of the ARR. A violation of the main propeller subsystem constraint results in a violation of the ARR_1 of Table 2, therefore faults on the main propeller subsystems are isolable. Therefore every subsystem is detectable but only the main propeller subsystem is also isolable.

4.2.2. Parity space approach

Residuals for the fault diagnosis system are obtained by applying the parity space approach, that is a model-based technique for linear systems to obtain residuals which are independent from disturbances and the initial state of the system. Assuming as measured output the ship velocity $\boldsymbol{\nu}_{LF}$, the linearization of the ship dynamics model in (17) around $\boldsymbol{\eta}_{LF}=\mathbf{0}$ and $\boldsymbol{\nu}_{LF}=\mathbf{0}$ gives a linear continuous-time state-space model in the form

$$\dot{\boldsymbol{\nu}}_{\mathrm{LF}}=-\boldsymbol{M}^{-1}\boldsymbol{D}\boldsymbol{\nu}_{\mathrm{LF}}+\boldsymbol{M}^{-1}\boldsymbol{T}\boldsymbol{u}+\boldsymbol{M}^{-1}\boldsymbol{T}\boldsymbol{d}+\boldsymbol{M}^{-1}\boldsymbol{T}\boldsymbol{f},\ \boldsymbol{y}=\boldsymbol{\nu}_{\mathrm{LF}},\quad \boldsymbol{\nu}_{\mathrm{LF}}(0)=\mathbf{0} \tag{28}$$

where the failure of a thruster is modeled as an additive fault.

A model of this type can also be written in terms of transfer functions:

$$\boldsymbol{y}=\boldsymbol{H}_{\mathrm{yu}}(s)\boldsymbol{u}(s)+\boldsymbol{H}_{\mathrm{yd}}(s)\boldsymbol{d}(s)+\boldsymbol{H}_{y\boldsymbol{\nu}_{\mathrm{LF}}}(s)\boldsymbol{\nu}_{\mathrm{LF}}(0)+\boldsymbol{H}_{\mathrm{yf}}(s)\boldsymbol{f}(s) \tag{29}$$

where

$$\begin{aligned}
\boldsymbol{H}_{yu}(s)&=\left(s\boldsymbol{I}+\boldsymbol{M}^{-1}\boldsymbol{D}\right)^{-1}\boldsymbol{M}^{-1}\overline{\boldsymbol{T}}\\
\boldsymbol{H}_{y\boldsymbol{\nu}_{LF}}(s)&=\left(s\boldsymbol{I}+\boldsymbol{M}^{-1}\boldsymbol{D}\right)^{-1}\\
\boldsymbol{H}_{yd}(s)&=\left(s\boldsymbol{I}+\boldsymbol{M}^{-1}\boldsymbol{D}\right)^{-1}\boldsymbol{M}^{-1}\overline{\boldsymbol{T}}\\
\boldsymbol{H}_{yf}(s)&=\left(s\boldsymbol{I}+\boldsymbol{M}^{-1}\boldsymbol{D}\right)^{-1}\boldsymbol{M}^{-1}\overline{\boldsymbol{T}}
\end{aligned} \tag{30}$$

As stated in Blanke et al. (2006), a residual generator is a filter with input $\boldsymbol{u}$ and $\boldsymbol{y}$. As with the supervision of a linear time-invariant system in (28), the class of considered filters is restricted to linear time-invariant systems of the following transfer function form, assuming zero initial conditions:

$$\boldsymbol{r}_{psa}(s)=\boldsymbol{V}_{ru}(s)\boldsymbol{u}(s)+\boldsymbol{V}_{ry}(s)\boldsymbol{y}(s)=\begin{pmatrix}\boldsymbol{V}_{ru}(s) & \boldsymbol{V}_{ry}(s)\end{pmatrix}\begin{pmatrix}\boldsymbol{u}(s)\\ \boldsymbol{y}(s)\end{pmatrix} \tag{31}$$

Table 2
Dependability matrix.

Subsystem	Main propeller	Tunnel thrusters	Azimuth thrusters
ARR_1	×		
ARR_2		×	×
ARR_3		×	×

Then the problem of residual generator design can be stated as follows:

Problem 1. Finding a stable linear time-invariant system in (31) such that

- In the absence of fault $\boldsymbol{f}(t)=0$ for all t, the output signal $\boldsymbol{r}_{\mathrm{psa}}(t), t>0$ asymptotically decays to zero for any input $\boldsymbol{u}(t), \boldsymbol{d}(t), t>0$ and any initial conditions $\boldsymbol{\nu}_{LF}(0)$.
- $\boldsymbol{r}_{psa}(t)$ is affected by $\boldsymbol{f}(t)$.

As stated in Blanke et al. (2006), to determine the conditions to be fulfilled by $\boldsymbol{V}_{ru}(s)$ and $\boldsymbol{V}_{ry}(s)$ for (31) to be a residual generator, (29) is substituted in (31) obtaining the following:

$$\boldsymbol{r}_{\mathrm{psa}}(s)=\begin{pmatrix}\boldsymbol{V}_{\mathrm{ru}}(s)+\boldsymbol{V}_{\mathrm{ry}}(s)\boldsymbol{H}_{\mathrm{yu}}(s) & \boldsymbol{V}_{\mathrm{ry}}(s)\boldsymbol{H}_{\mathrm{yd}}(s)\end{pmatrix}\begin{pmatrix}\boldsymbol{u}(s)\\ \boldsymbol{d}(s)\end{pmatrix} + \boldsymbol{V}_{\mathrm{ry}}(s)\boldsymbol{H}_{y_{\nu_{\mathrm{LF}}}}(s)\nu_{\mathrm{LF}}(0)+\boldsymbol{V}_{\mathrm{ry}}(s)\boldsymbol{H}_{\mathrm{yf}}(s)\boldsymbol{f}(s) \tag{32}$$

Fulfillment of the conditions of Problem 1 requires

$$\begin{pmatrix}\boldsymbol{V}_{ru}(s)+\boldsymbol{V}_{ry}(s)\boldsymbol{H}_{yu}(s) & \boldsymbol{V}_{ry}(s)\boldsymbol{H}_{yd}(s)\end{pmatrix}=\boldsymbol{O} \tag{33}$$

which can be rewritten as

$$\begin{pmatrix}\boldsymbol{V}_{ry}(s) & \boldsymbol{V}_{ru}(s)\end{pmatrix}\underbrace{\begin{pmatrix}\boldsymbol{H}_{yu}(s) & \boldsymbol{H}_{yd}(s)\\ \mathbf{I} & \boldsymbol{O}\end{pmatrix}}_{\boldsymbol{H}(s)}=\boldsymbol{O} \tag{34}$$

Calling $\boldsymbol{p}(s)$ the least common multiple of the denominators of the entries of $\boldsymbol{V}_{ru}(s)$ and $\boldsymbol{V}_{ry}(s)$, the left most matrix in (34) can be written:

$$\begin{pmatrix}\boldsymbol{V}_{\mathrm{ry}}(s) & \boldsymbol{V}_{\mathrm{ru}}(s)\end{pmatrix}=\frac{\begin{pmatrix}\overline{\boldsymbol{V}}_{\mathrm{ry}}(s) & \overline{\boldsymbol{V}}_{\mathrm{ru}}(s)\end{pmatrix}}{\boldsymbol{p}(s)} \tag{35}$$

where $\overline{\boldsymbol{V}}_{ry}(s)$ and $\overline{\boldsymbol{V}}_{ru}(s)$ are suitable polynomial matrices. Hence the class of filters that fulfill (34) is the set of polynomial matrices that lie in the left null space of $\boldsymbol{H}(s)$. Let $\boldsymbol{F}(s)$ be a matrix in which rows form an irreducible polynomial basis for the rational vector null space of $\boldsymbol{H}(s)$, then the matrix $\begin{pmatrix}\overline{\boldsymbol{V}}_{ry}(s) & \overline{\boldsymbol{V}}_{ru}(s)\end{pmatrix}$ is obtained by combinations of the rows of $\boldsymbol{F}(s)$, namely

$$\begin{pmatrix}\boldsymbol{V}_{\mathrm{ry}}(s) & \boldsymbol{V}_{\mathrm{ru}}(s)\end{pmatrix}=\boldsymbol{Q}(s)\boldsymbol{F}(s) \tag{36}$$

where $\boldsymbol{Q}(s)$ is an arbitrary polynomial matrix with appropriate number of columns. Then, substituting (36) into (35), the following is obtained:

$$\begin{pmatrix}\boldsymbol{V}_{\mathrm{ry}}(s) & \boldsymbol{V}_{\mathrm{ru}}(s)\end{pmatrix}=\frac{\boldsymbol{Q}(s)\boldsymbol{F}(s)}{\boldsymbol{p}(s)} \tag{37}$$

Introducing (37) into (31) finally results in

$$\boldsymbol{r}_{\mathrm{psa}}(s)=\frac{\boldsymbol{Q}(s)\boldsymbol{F}(s)}{\boldsymbol{p}(s)}\begin{pmatrix}\boldsymbol{u}(s)\\ \boldsymbol{y}(s)\end{pmatrix} \tag{38}$$

where the filter described in (38) is a residual generator. The choice of the matrix $\boldsymbol{Q}(s)$ is made in order to ensure filtering of high frequency disturbances which always exist, even though they were not considered in the model (29). Three residuals are found using the considered parity space method, namely r_{psa_j}, where $j\in 1,2,3$. The terms f_i refers to a fault in the i-th thruster, with $i\in 1,2,..,6$, for the considered offshore supply vessel of Fig. 2. The dependency matrix which links residuals to the faults is shown in Table 3. As a consequence of the symmetry of the actuator system, the results in Table 3 are equal in pairs in nominal conditions. When a fault occurs on the actuators, one of the subsystems does not verify the constraints, because in this case the two actuator torques of the pair are different in the faulty case.

Table 3
Dependency matrix.

Residual	f_1	f_2	f_3	f_4	f_5	f_6
r_{psa_1}	×	×	0	0	×	×
r_{psa_2}	0	0	×	×	×	×
r_{psa_3}	×	×	×	×	×	×

4.2.3. Luenberger observer

To solve the fault isolation problem the Luenberger observer is proposed to find other residuals (Luenberger, 1971). According to the introduced notations, the DP ship linear model in (28), without considering environmental disturbances and faults, has the following form:

$$\dot{\boldsymbol{\nu}}_{LF}=\underbrace{-\boldsymbol{M}^{-1}\boldsymbol{D}}_{\boldsymbol{A}}\boldsymbol{\nu}_{LF}+\underbrace{-\boldsymbol{M}^{-1}\overline{\boldsymbol{T}}}_{\boldsymbol{B}}\boldsymbol{u},\qquad \boldsymbol{y}=\boldsymbol{\nu}_{LF}. \tag{39}$$

The Luenberger state estimate takes the form

$$\dot{\hat{\boldsymbol{\nu}}}_{LF}=(\boldsymbol{A}-\boldsymbol{G})\hat{\boldsymbol{\nu}}_{LF}+\boldsymbol{B}\boldsymbol{u}+\boldsymbol{G}\boldsymbol{y}, \tag{40}$$

where $\boldsymbol{G}$ is a matrix chosen so that the eigenvalues of $(\boldsymbol{A}-\boldsymbol{G})$ are in the left-half complex plane. The residuals are calculated as the difference between the measured and the estimated velocity:

$$\boldsymbol{r}_{Lue}(t)=\boldsymbol{\nu}-\hat{\boldsymbol{\nu}}. \tag{41}$$

4.3. Change detection

To impose robustness the cumulative sum (*CUSUM*) change detector is implemented. To identify faults causing changes in the mean of the residuals, without changing their standard deviation, the cumulative sum algorithm introduced in Basseville and Nikiforov (1993) is proposed for improving the robustness of the fault detection system. Denoting with r_k the residual value at the time k, μ_0 and σ^2 as the mean and variance, respectively, of the residual and $\delta\mu$ as the change in the mean, the decision function g_k^+ is

$$g_k^+=\frac{\delta\mu}{\sigma^2}\max\left(0, g_{k-1}^+ + r_k-\mu_0-\frac{\delta\mu}{2}\right). \tag{42}$$

The decision function g_k^+ is evaluated against a threshold h to trigger an alarm. The implementation of the *CUSUM* algorithm requires a knowledge of the mean value of the residual after the fault which may be overestimated, as stated in Blanke et al. (2006). The threshold h is a trade-off between the delay in identifying the fault and the false alarm frequency. The *CUSUM* algorithm is applied to the residual obtained using the parity space approach and the Luenberger observer approach. If the decision function is greater than the threshold h, the alarm for the respective residual is triggered as described in Table 4, where the components of the alarm vector

$$\boldsymbol{alm}=[alm_{PSA_1}, alm_{PSA_2}, alm_{PSA_3}, alm_{Leu_1}, alm_{Leu_2}, alm_{Leu_3}]^T$$

are correlated with the considered faults f_i, with $i=1,2,\ldots,6$.

4.4. Fault isolation

The proposed fault isolation model allows the faulty thruster to be identified by combining the results of the change detection algorithm applied on the residuals processed by the parity space approach and the Luenberger observer. The proposed fault isolation logic is described in Fig. 14 and Table 4, where the i-th fault is isolated when the alarm *alm* vector has the value given in the i-th column.

As an example, a fault on the main propeller (thruster number 1) is isolated when $alm_{PSA_1}=1$ and $alm_{Leu_2}=1$ while $alm_{PSA_2}=$

Table 4
Isolation logic.

Alarm	f_1	f_2	f_3	f_4	f_5	f_6
alm_{PSA_1}	1	1	0	0	0	0
alm_{PSA_2}	0	0	1	1	0	0
alm_{PSA_3}	0	0	0	0	1	1
alm_{Leu_1}	0	1	1	0	0	0
alm_{Leu_2}	1	0	0	1	1	1
alm_{Leu_3}	1	1	1	1	1	1

$alm_{PSA_3} = alm_{Leu_1} = 0$ and $alm_{PSA_1} = 1$ or 0. The isolation table in Table 4 shows that the alm_{Leu_3} does not give any informations about faults isolation being triggered in any case; the yaw angle is affected in any case by an actuator fault. Thus that information is not used for isolation. It is also worth noting that faults affecting the two azimuthal thrusters cannot be isolated: when $alm_{PSA_3} = 1$ and $alm_{Leu_2} = 1$ a fault affecting either one or two azimuth thrusters is confirmed, but there is no indication of which one is faulty. To overcome this problem a solution is proposed in Section 6.4.

5. Discrete-Time Variable Structure Control

A Discrete-Time Variable Structure Control (DTVSC) (Utkin, 1992; Furuta, 1990; Corradini et al., 2012; Corradini and Orlando, 1997; Chakrabarty and Bandyopadhyay, 2015; Khandekar et al., 2013) is considered which allows an appropriate formulation of the problem in a sampled-data system context, which is doubtless useful in view of the practical discrete-time implementation on the digital computer of a real DP control system. The DTVSC proposed in this paper considers the control of the ship position $\boldsymbol{\eta}$ by using the velocities $\boldsymbol{\nu}_{LF}$ in the $\{b\}$ frame. The system model is derived from (17) and takes the following form:

$$\dot{\nu}_{\mathrm{LF}} = -\boldsymbol{M}^{-1}\boldsymbol{D}\boldsymbol{\nu}_{\mathrm{LF}} - \boldsymbol{M}^{-1}\boldsymbol{R}(\psi)\boldsymbol{b} + \boldsymbol{M}^{-1}\overline{\boldsymbol{T}}\boldsymbol{u} + \boldsymbol{M}^{-1}\overline{\boldsymbol{T}}\boldsymbol{d} + \boldsymbol{M}^{-1}\overline{\boldsymbol{T}}\boldsymbol{f}. \tag{43}$$

The discretization of the model equation (43) with a sampling time T_s, and zero order hold with period T_s, according to standard techniques gives

$$\begin{aligned}\boldsymbol{\nu}_{\mathrm{LF}}(k+1) = {} & \underbrace{\mathrm{e}^{-\boldsymbol{M}^{-1}\boldsymbol{D}T_s}}_{\boldsymbol{F}}\boldsymbol{\nu}_{\mathrm{LF}}(k) \\ & + \underbrace{\int_0^{T_s}\mathrm{e}^{-\boldsymbol{M}^{-1}\boldsymbol{D}\sigma}\boldsymbol{M}^{-1}\,\mathrm{d}\sigma}_{\boldsymbol{G}}\boldsymbol{u}(k) - \underbrace{\int_0^{T_s}\mathrm{e}^{-\boldsymbol{M}^{-1}\boldsymbol{D}\sigma}\boldsymbol{M}^{-1}\boldsymbol{R}(\psi(\sigma))\boldsymbol{b}(\sigma)\,\mathrm{d}\sigma}_{\boldsymbol{G}_b} \\ & + \underbrace{\int_0^{T_s}\mathrm{e}^{-\boldsymbol{M}^{-1}\boldsymbol{D}\sigma}\boldsymbol{M}^{-1}\overline{\boldsymbol{T}}\boldsymbol{d}(\sigma)\,\mathrm{d}\sigma}_{\boldsymbol{G}_d} + \underbrace{\int_0^{T_s}\mathrm{e}^{-\boldsymbol{M}^{-1}\boldsymbol{D}\sigma}\boldsymbol{M}^{-1}\overline{\boldsymbol{T}}\boldsymbol{f}(\sigma)\,\mathrm{d}\sigma}_{\boldsymbol{G}_f}.\end{aligned} \tag{44}$$

Denoting the control generalized force vector in a body-fixed $\{b\}$ frame as

$$\boldsymbol{\tau}^*(k) = [\tau_u^*(k)\tau_v^*(k)\tau_r^*(k)]^T = \boldsymbol{G}\boldsymbol{u}(k) \tag{45}$$

the discrete-time model used for deriving the control law takes the form

$$\boldsymbol{\nu}_{\mathrm{LF}}(k+1) = \boldsymbol{F}\boldsymbol{\nu}_{\mathrm{LF}}(k) + \boldsymbol{\tau}^*(k) + \boldsymbol{G}_b(k) + \boldsymbol{G}_d(k) + \boldsymbol{G}_f(k). \tag{46}$$

It is assumed that model parameters may differ from their nominal values for some unknown but bounded quantities $\boldsymbol{\Delta F}$:

$$\boldsymbol{F} = \overline{\boldsymbol{F}} + \boldsymbol{\Delta F}, \tag{47}$$

Moreover, the thruster failures $\boldsymbol{G}_f(k)$ are considered bounded by known quantities $\boldsymbol{\Delta}G_f$; the thruster torques are limited by the maximum torque value and the fault is considered to be a value from 0 to 100% of the maximum thruster torque. It is also assumed that the slowly varying environmental and input disturbances ($\boldsymbol{G}_b$ and $\boldsymbol{G}_d$, respectively) are limited by the known quantities $\boldsymbol{\Delta}G_b$ and $\boldsymbol{\Delta}G_d$, respectively. These quantities have been chosen considering the value of the bias $\boldsymbol{b}$ of Eq. (11) for $\boldsymbol{\Delta}G_b$ and the value of the bias $\boldsymbol{d}$ of Eq. (17) for $\boldsymbol{\Delta}G_d$.

Defining the following discrete-time sliding surfaces:

$$\underbrace{\begin{bmatrix} s_u(k) \\ s_v(k) \\ s_r(k) \end{bmatrix}}_{\boldsymbol{s}(k)} = \boldsymbol{\Delta\nu}_{LF}(k) + \underbrace{\begin{bmatrix} \lambda_u & 0 & 0 \\ 0 & \lambda_v & 0 \\ 0 & 0 & \lambda_r \end{bmatrix}}_{\boldsymbol{\Lambda}} \boldsymbol{\Delta\nu}_{LF}(k-1) = 0 \tag{48}$$

where $\lambda_u, \lambda_v, \lambda_r \in (-1, 1)$ and $\boldsymbol{\Delta\nu}_{LF}(k) = \boldsymbol{\nu}_{LF}(k) - \boldsymbol{\nu}_{LF}^*(k)$ with $\boldsymbol{\nu}_{LF}^*(k)$ being the given reference value for the velocity.

Using standard techniques such as Corradini et al. (2012), it can be verified that a quasi-sliding motion on the surfaces $\boldsymbol{s}(k) = 0$ of (48) is ensured by the control law

$$\boldsymbol{\tau}^*(k) = \boldsymbol{\tau}_{eq}^*(k) + \boldsymbol{\tau}_n^*(k) \tag{49}$$

where the equivalent control is given by

$$\boldsymbol{\tau}_{eq}^*(k) = \boldsymbol{\nu}_{LF}(k) - \overline{\boldsymbol{F}}\boldsymbol{\nu}_{LF}(k) - \boldsymbol{\Lambda}\boldsymbol{\Delta\nu}_{LF}(k) \tag{50}$$

and the discontinuous control term $\boldsymbol{\tau}_n = \left[\tau_{n_u}^*\ \tau_{n_v}^*\ \tau_{n_r}^*\right]^T$ is given by

$$\tau_{n_i}^*(k) = \begin{cases} \vartheta_i\left(|s_i(k)| - \varrho_i\right) & \text{if} \quad |s_i(k)| > \varrho_i \\ -s_i(k) + \tau_{n_i}^*(k-1) & \text{if} \quad |s_i(k)| \le \varrho_i \end{cases}, \quad i \in \{u, v, r\} \tag{51}$$

with parameters $|\vartheta_i| < 1$ with $i \in \{u, v, r\}$ and $\boldsymbol{\varrho} = \left[\varrho_u\ \varrho_v\ \varrho_r\right]^T$ given by

$$\boldsymbol{\varrho} = \boldsymbol{\Delta F}\boldsymbol{V} + \boldsymbol{\Delta G}_b + \boldsymbol{\Delta G}_d + \boldsymbol{\Delta}G_f + \boldsymbol{\varrho}^* \tag{52}$$

where $\boldsymbol{V}$ and $\boldsymbol{\varrho}^*$ are the vectors of the maximum generalized speed and acceleration, respectively, during DP operation.

Moreover, integral action for drift force compensation is used to minimize the steady-state position error $\boldsymbol{\Delta\eta}$, as stated in Loria et al. (2000):

$$\boldsymbol{\tau}_I(k) = \boldsymbol{\tau}_I(k-1) + K_I T_s(\boldsymbol{\eta}_{LF}^*(k-1) - \boldsymbol{\eta}_{LF}(k-1)). \tag{53}$$

To obtain zero steady-state errors, it is possible to sum the integral action (53) to DTVSC in the control law, see Fossen (2011). The final control law is given by combining the DTVSC and the integral actions:

$$\boldsymbol{\tau}_c(k) = \boldsymbol{\tau}^*(k) + \boldsymbol{\tau}_I(k). \tag{54}$$

5.1. System reconfiguration

Fault handling incorporates a reconfiguration module which can be recovered from the actuator faults. The system reconfiguration algorithm includes strategies for n-different thruster failure scenarios. As shown in Fig. 4, the system reconfiguration is applied by reallocating the thrust force demand using the control law in (54) and choosing a proper controller c_i, where control parameters ϑ_i and $\boldsymbol{\Lambda}$ are pre-computed for the thruster failure f_i. The system reconfiguration logic uses the results of the fault diagnosis to enable the appropriate controller c_i to handle the fault f_i, as reported in Table 4. Therefore the system reconfiguration architecture comprises a bank of $n=6$ controllers, one for each possible fault. In nominal conditions, the controller c_0 allocates the same thrust on each pair of actuators. This is due to the symmetry of the thrusters with to respect to the ship geometry, as described in Section 2.3.2:

$$\begin{aligned} & \boldsymbol{G}\boldsymbol{u}(k) = \boldsymbol{\tau}^{*(0)}(k) + \boldsymbol{\tau}_I^{(0)}(k) \\ & u_i(k) = u_{i+1}(k) \quad \text{for} \quad i = 1, 3, 5. \end{aligned} \tag{55}$$

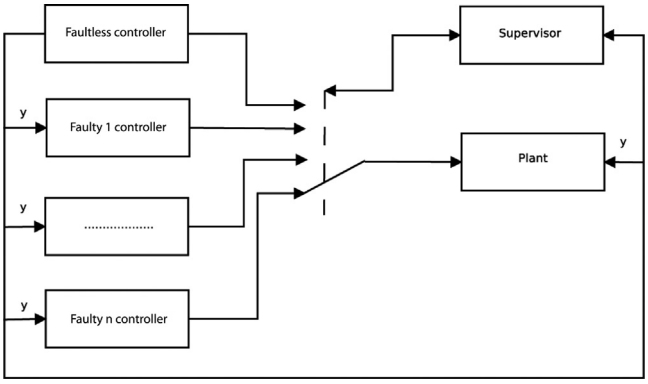

Fig. 4. System reconfiguration architecture.

When a fault is detected on the i-th thruster the relative thrust force u_i is set to zero (complete loss) or to a constant value $\overline{u}_i$ (stall), the controller c_i is applied and the following equation system is considered for the reallocation:

$$\begin{aligned} &\boldsymbol{Gu}(k) = \boldsymbol{\tau}^{*(i)}(k) + \boldsymbol{\tau}_l^{(i)}(k) \\ &u_i = 0 \quad \text{or} \quad \overline{u}_i \\ &u_m(k) = u_l(k) \quad \text{for} \quad m = 1,3,5 \wedge m \neq i \quad l = 2,4,6 \wedge l \neq i. \end{aligned} \tag{56}$$

6. Simulation results

In this section the results of the simulations are presented. The DTVSC is compared with a standard PID controller proposed in Fossen and Perez (2010). Kalman filter-based observers are tested against a Passive Nonlinear Observer from Strand and Fossen (1999). The *MSS* toolbox proposed in Fossen and Perez (2010) was used for the simulations. This toolbox provides a PID controller, whose parameters are chosen using an LQR algorithm (Fossen, 2011) and a Passive Nonlinear Observer, whose notch frequency is tuned by Strand and Fossen (1999) to correspond to the wave peak frequency. On the contrary the DTVSC was designed by the authors and implemented in the MSS. The dynamic model of the CyberShip 2 (CS2) is considered for simulations. This is a 1:70 scale model of an offshore supply vessel with a mass of 15 kg and a length of 1.255 m. The maximum surge force is 2.0 N, the maximum sway force is 1.5 N, while the maximum yaw moment is 1.5 N m. This ship is located in the Marine Cybernetics Laboratory (MCLab) at the Norwegian University of Science and Technology. For more details about the CS2 see Skjetne et al. (2004).

The mean Integral of Squared Error (*ISE*) is considered to obtain a quantitative comparison between the results of different simulations. This is a commonly used performance index in control and estimation theory. For the DP system the indices depend on the error between the reference position and orientation and the position and orientation measured by the sensors, i.e. $\boldsymbol{\Delta\eta}$. The mean ISE index expression, normalized with respect to the time length of the simulation, is

$$ISE : \frac{1}{T}\int_{t_0}^{t_f} \boldsymbol{\Delta\eta}(t)^2 \, \mathrm{d}t. \tag{57}$$

The following expression is the percentage variation of the ISE index when comparing PID and DTVSC performances:

$$\%ISE : \frac{ISE_{DTVSC} - ISE_{PID}}{ISE_{PID}} \cdot 100. \tag{58}$$

6.1. Filters comparison

The Extended Kalman Filter (EKF), the Multi-rate Kalman Filter (MREKF) and the Passive Nonlinear Observer (PNLO) are compared, using the DTVS controller in a test of 2000 s to evaluate which wave filtering technique has to be used. The sea conditions are described by a significant wave height of $H_s = 0.8$ m and a wave period of $T_0 = 7.85$ s. The PNLO is tuned up using dominating wave frequency 0.8 rad/s as the notch frequency. Results are shown in Fig. 5. The upper figure shows how the position estimation based on the EKF (red dashed line), the MREKF (blue dotted line) and the PNLO (green dash-dotted line) matches the surge displacement reference. The lower figure shows the comparison of the variances in control inputs in order to quantitatively evaluate the performance of the three filters: Extended Kalman Filter (red dashed line), Multi-rate Kalman Filter (blue dotted line) and Passive Nonlinear Observer (green dash-dotted line). The PNLO shows worse performance with respect to the other filters in terms of required control effort amplitudes: when the PNLO is used for position estimation control input amplitudes are much (up to 55%) larger than the ones required when using the EKF or MREKF by comparing the variance in generalized control inputs in Table 5.

To choose between EKF and MREKF the Root Mean Squared Error (RMSE) of state estimation is evaluated in Table 6 and results show that MREKF shows better performances. Considering that the EKF and the MREKF have comparable performance, but that the MREKF can also take into account differences in sensor sampling frequency, the MREKF is chosen as the reference filter for evaluating the controller performances in Section 6.2.

6.2. Controllers comparison

Simulations have a total period of 2000 s and are divided into two successive stages. In the first stage the dynamic positioning system must maintain the vessel fixed to the initial position ($\boldsymbol{\eta}^* = \{0\text{ m}, 0\text{ m}, 0^\circ\}$), despite the environmental disturbances from waves, wind and currents. In the second stage the dynamic positioning system takes the ship to a different position ($\boldsymbol{\eta}^* = \{20\text{ m}, 20\text{ m}, 50^\circ\}$). To avoid abrupt acceleration, due to the

Table 5
Variance in generalized forces for different filtering techniques.

Filter	τ_u	τ_v	τ_r
PNLO	0.0071	0.0371	$3.3797 \cdot 10^{-5}$
EKF	0.0061	0.0249	$0.0249 \cdot 10^{-5}$
MREKF	0.0061	0.0251	$1.8658 \cdot 10^{-5}$

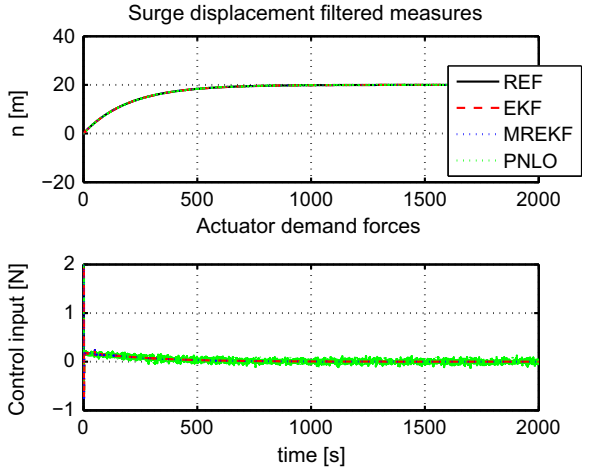

Fig. 5. (Upward) plot of the reference and estimated path for surge displacement. (Downward) control input. (For interpretation of the references to color in this figure, the reader is referred to the web version of this paper.)

change in reference position, a reference path with a smooth position change was used. The reference path and the two stages in the simulations are shown as black solid line in Fig. 6. The first and second stages are referred to as the constant references and the varying references condition, respectively. The PID and DTVS controllers are compared using the Multi-rate Extended Kalman Filter. Performance is compared in both the first and second stages, when the references are constant and when the references are varying, respectively. The results are shown in Fig. 6 and the performance index is reported in Table 7. Simulations show that the DTVSC and the PID controller have the same performances when the dynamic positioning system is being used to maintain a fixed reference position. However the DTVSC performs better than the PID control when the position reference changes, showing significantly smaller overshoots during the transition. This is reflected in a smaller ISE performance index considering the second stage of simulations with varying references (see Table 7). Therefore lower tracking errors are obtained using the DTVSC for the DP system.

6.3. Disturbances and parametric variations

To show the DTVSC robustness, variations in the model parameters and input disturbances are considered. In the first set of simulations, a 20% increase in the inertia value is considered. The results are shown in Table 8. To test robustness to input disturbances, a torque input disturbance affecting one main propeller (u_1) with a magnitude equal to 30% of the maximum value is considered. The results are shown in Fig. 7: reference (black solid line); estimated positions in the local geographical $\{n\}$ frame using the DTVSC (red dotted line) and the PID controller (blue dash-dotted line). The results are summarized in Table 9. In both cases, the DTVS controller has better performance with respect to the PID controller, both when the references are constant and when the references are varying. Therefore the DTVSC proves to be robust with respect to input disturbances and to parametric variations. Fig. 8 shows the convergence of the sliding surfaces confirming the robustness of the proposed control approach.

6.4. Faults during transients

This simulation tests the system when a fault affects a tunnel thruster at time instant 200 s, while the ship is reaching the desired position, as shown in Fig. 11. The fault detection system identifies the fault, the supervisor analyzes the alarm signals given by the CUSUM algorithm output for the residuals calculated using the parity space approach (see Fig. 9(b)) and using the Luenberger observer (see Fig. 9(b)), and chooses the correct controller.

Table 6
RMSE using different filtering techniques.

Generalized position	PNLO	EKF	MREKF
n (m)	0.0231	0.0043	0.0032
e (m)	0.0268	0.0087	0.0071
ψ (deg)	0.4177	0.0558	0.0267

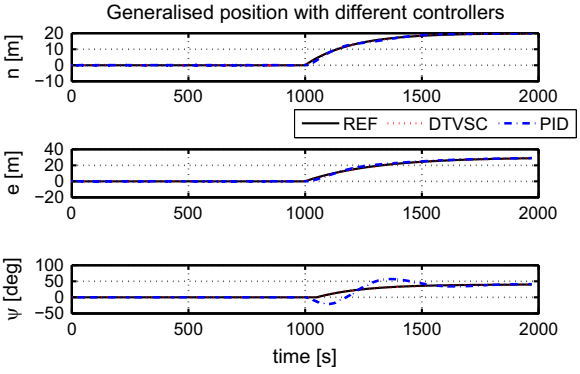

Fig. 6. Generalized position with the considered controllers. Reference (black solid line) and estimated positions in the local geographical $\{n\}$ frame using DTVSC (red dotted line) and the PID controller (blue dash-dotted line). The surge displacement n, sway displacement e and heading ψ are shown in the figures from up to down. (For interpretation of the references to color in this figure caption, the reader is referred to the web version of this paper.)

Table 7
ISE performance comparison between DTVSC and the PID controller. Both the constant references and the varying references conditions are considered.

Generalized position	Constant references			Varying references		
	DTVSC	PID	% ISE	DTVSC	PID	% ISE
n	0.0291	0.0291	1.23E−3	0.0580	0.8917	84
e	0.0291	0.0291	1.22E−3	0.0582	0.7293	92
ψ	$6\cdot10^{-5}$	$6\cdot10^{-5}$	1.22E−3	0.0001	0.0623	99

Table 8
ISE performance comparison between DTVSC and the PID controller with a 20% increase in the inertia of the vessel. Both the constant references and the varying references conditions are considered.

Generalized position	Constant references			Varying references		
	DTVSC	PID	% ISE	DTVSC	PID	% ISE
n	0.032	0.13	75	0.072	0.38	81
e	0.031	0.19	83	0.07	0.72	90
ψ	$7\cdot10^{-5}$	$7\cdot10^{-4}$	90	$1.7\cdot10^{-4}$	0.06	99

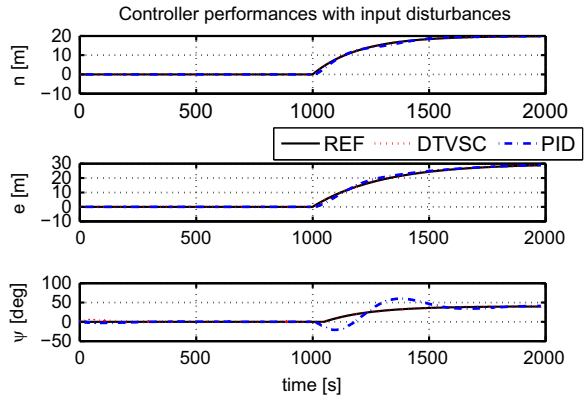

Fig. 7. Generalized position with the considered controllers in case of a torque input disturbance.

Table 9
ISE performance comparison between DTVSC and the PID controller with a torque input disturbance affecting u_1 . Both the constant references and the varying references conditions are considered.

Generalized position	Constant references			Varying references		
	DTVSC	PID	% ISE	DTVSC	PID	% ISE
n	0.0874	0.1285	34	0.1187	0.4771	75
e	0.0354	0.1841	80	0.0666	0.8056	92
ψ	0.0023	0.0028	17	0.0036	0.1226	97

In this simulation, the supervisor isolates the fault and changes from faultless c_0 to c_3 controller at time instant 208 s, as shown in Fig. 10(a). Control system performances are shown in Fig. 12, where the generalized position error suddenly increases after the fault event. The c_3 controller is enabled after 8 s and thrust force is reallocated among other non-faulty thrusters and the position error slowly decays to zero. Summarizing the fault diagnosis and the control reconfiguration system, it is possible to detect and isolate the fault, switch to the appropriate controller in 8 s and drive the position error towards zero. Fault occurring on azimuth thrusters is a particular case, because it is possible to detect a fault on these thrusters, but the thruster affected by the failure cannot be isolated. Therefore the fault detection module gives a generic alarm in case of faults on the azimuth thruster. The supervisor assigns one of the two controllers (c_5 or c_6) relative to the two azimuth thrusters and evaluates the error between the references and the measured values. If this error is greater than a threshold, the fault is on the other azimuth thruster and the supervisor switches to the correct controller, as can be seen in Fig. 10(b). The supervisor logic detects the fault and switch the controller at 218 s, fault isolation and another controller switch occurs at 250 s. The fault diagnosis system can identify and isolate the fault and choose the correct controller in 50 s, which is a reasonable time compared to the typical time constants of DP systems.

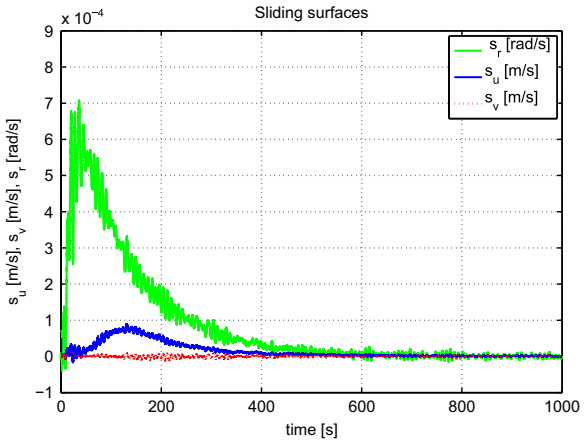

Fig. 8. Sliding surface dynamics.

6.5. Faults in steady state

To investigate control performances in steady state, a simulation was performed with a fault occurring when the initial transients are

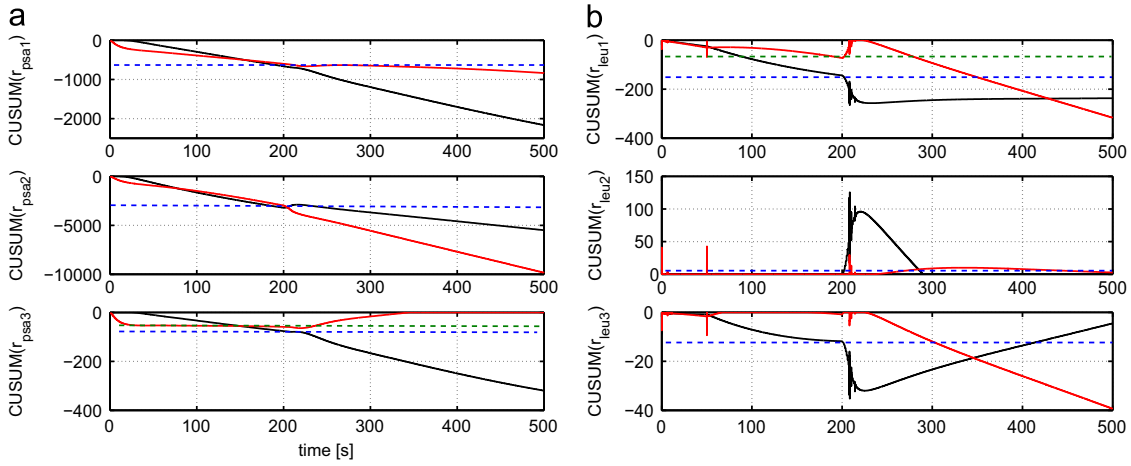

Fig. 9. Tunnel truster failure. Change detection algorithm outputs are solid red and black lines. Thresholds are blue and green dashed lines (a) Parity Space Approach (b) Luenberger Observer. (For interpretation of the references to color in this figure caption, the reader is referred to the web version of this paper.)

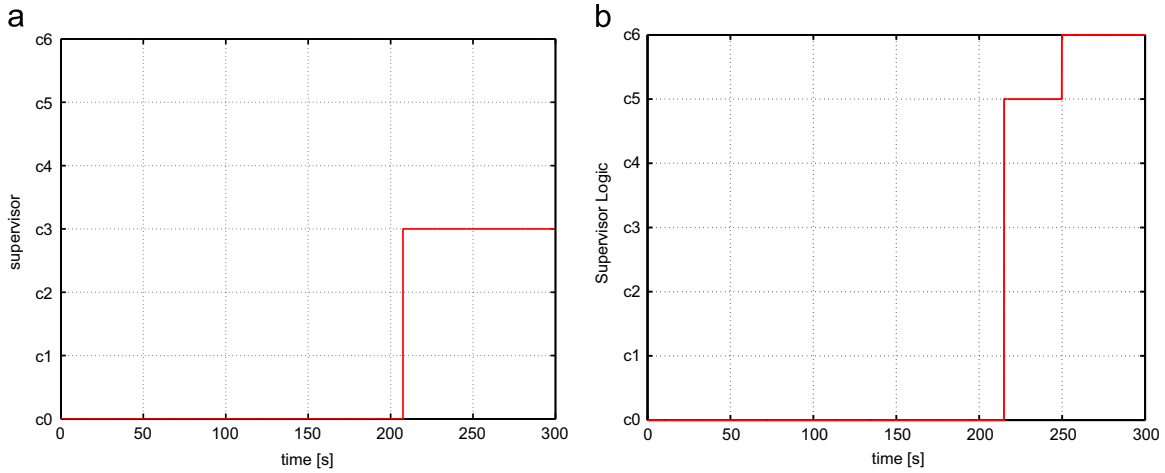

Fig. 10. Left: tunnel thruster 1 failure. Right: azimuth thruster failure. Supervision logic select first the fifth controller c_5, after a short evaluation, switches to c_6 (a) Tunnel thruster failure (b) Azimuth thruster failure.

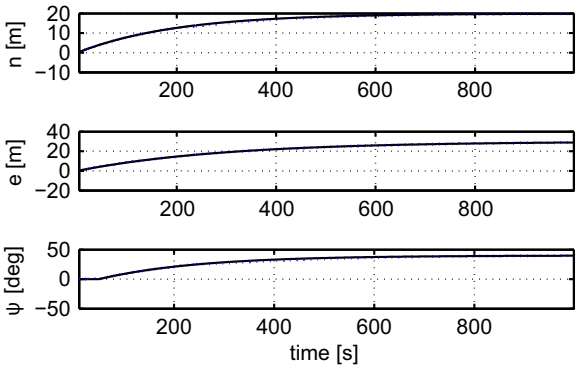

Fig. 11. Generalized position in case of a tunnel thruster failure. Reference (black solid line) and estimated (blue dashed line) positions in the local geographical $\{n\}$ frame. (For interpretation of the references to color in this figure caption, the reader is referred to the web version of this paper.)

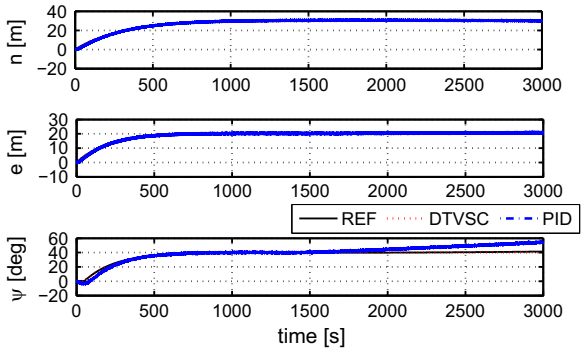

Fig. 13. Generalized position in case of a abrupt fault affecting one main propeller at 1200 s. Reference (black solid line) and estimated positions in the local geographical $\{n\}$ frame using DTVSC (red dotted line) and the PID control (blue solid line). (For interpretation of the references to color in this figure caption, the reader is referred to the web version of this paper.)

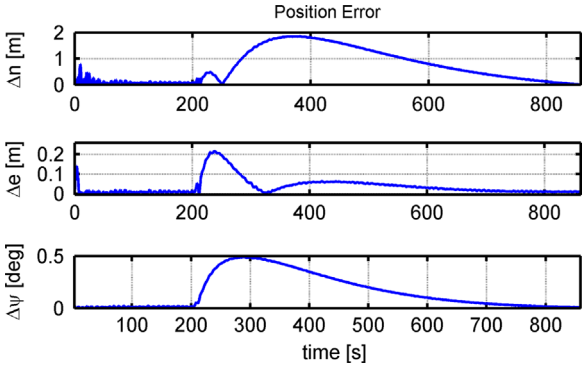

Fig. 12. Generalized position error with a tunnel thruster failure occurring at 200 s.

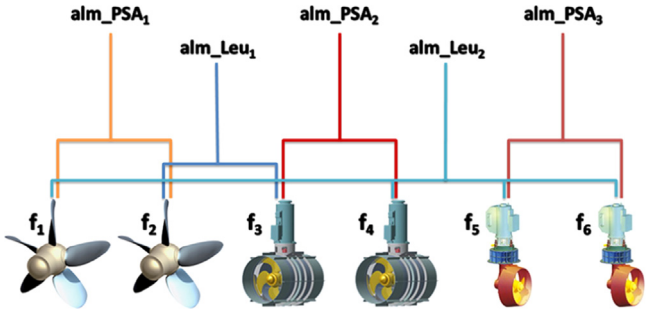

Fig. 14. Isolation logic.

expired. In this simulation the main propeller gets stuck at 1200 s; the fault amplitude equals the propeller torque at 1200 s. Fig. 13 shows the simulation results, comparing the PID and the DTVSC performance. Using the PID controller the surge (n) and sway (e) displacements are close to the reference values, but there is a drift in the ship heading (ψ) after the faults occur. This shows that the PID cannot handle a constant fault on a main propeller. Generalised position using the DTVSC shows no drift from the reference values, both before and after the faults occur, even before that the fault is isolated and identified. For this reason DTVSC proved to be more robust than PID control with respect to this kind of fault. When the fault diagnosis module identifies the fault, the supervision logic switches to the appropriate controller c_1, with slightly better performance than the default one c_0.

7. Conclusion

The problem of dynamic positioning plays a key role in all those cases in which it is not possible to anchor the ship to the seabed, or in which the ship position is bound to a specific point on the seafloor. In this paper, an architecture for the autonomous dynamic positioning of an offshore supply vessel is given using non-linear discrete control and wave filtering techniques. Simulations performed for the scale model (CS2) of an offshore supply vessel confirm the robustness of the control scheme in the presence of disturbances or parametric variations and show that DTVSC outperforms classic PID controllers both in case of nominal conditions and in the case of uncertainties and actuator disturbances. Three different wave filtering techniques were tested in the feedback loop. Simulations showed that the Extended Kalman filter and the Multi-rate Kalman Filter have comparable performances, but they outperform the standard Passive Nonlinear Observer in terms of variance in the controller efforts and drifts. The MREKF was preferred because it is designed for GPS and gyro-track signals which are acquired with different frequencies. A fault-tolerant architecture is also proposed using a bank of robust DTVS controllers and the MREKF wave filter. A comparison with a bank of PID controls optimized for every situation and operating condition has not been considered in this work because the DTVSC has proven to be more robust to environmental and input disturbances. Simulations show that the fault detection system identifies the fault, and the fault isolation system isolates the faulty component and chooses the correct controller and thruster allocation from a bank of DTVS controllers, designed considering faults on each actuator.

References

Balchen, J.G., Jenssen, N.A., Mathisen, E., Sælid, S., 1980. A dynamic positioning system based on Kalman filtering and optimal control. Model. Identif. Control 1 (3), 135–163.

Basseville, M., Nikiforov, I.V., 1993. Detection of Abrupt Changes—Theory and Application. Prentice Hall, Englewood Cliffs, NJ.

Benetazzo, F., Ippoliti, G., Longhi, S., Raspa, P., 2012. Discrete time variable structure control for the dynamic positioning of an offshore supply vessel. In: Preprints of the 2012 IFAC Workshop on Automatic Control in Offshore Oil and Gas Production, pp. 171–176.

Blanke, M., 2005. Diagnosis and fault-tolerant control for ship station keeping. In: Proceedings of the 2005 IEEE International Symposium on Intelligent Control, 2005. Mediterrean Conference on Control and Automation, pp. 1379–1384, June.

Blanke, M., Kinnaert, M., Lunze, J., Staroswiecki, M., 2006. Diagnosis and Fault Tolerant Control, 2nd edition Springer, Berlin.

Chakrabarty, S., Bandyopadhyay, B., 2015. A generalized reaching law for discrete time sliding mode control. Automatica 52, 83–86.

Chen, M., Ge, S.S., How, B., Choo, Y.S., 2013. Robust adaptive position mooring control for marine vessels. IEEE Trans. Control Syst. Technol. 21 (March (2)), 395–409.

Cocquempot, V., Izadi-Zamanabadi, R., Staroswiecki, M., Blanke, M., 1998. Residual generation for the ship benchmark using structural approach. In: UKACC International Conference on Control '98 (Conf. Publ. No. 455), vol. 2, pp. 1480–1485, September.

Corradini, M., Ippoliti, G., Longhi, S., Orlando, G., 2012. A quasi-sliding mode approach for robust control and speed estimation of PM synchronous motors. IEEE Trans. Ind. Electron. 59 (February (2)), 1096–1104.

Corradini, M.L., Orlando, G., 1997. A discrete adaptive variable-structure controller for MIMO systems, and its application to an underwater ROV. IEEE Trans. Control Syst. Technol. 5 (3), 349–359.

Donaire, A., Perez, T., 2012. Dynamic positioning of marine craft using a port-Hamiltonian framework. Automatica 48 (5), 851–856.

Fang, S., Blanke, M., Leira, B.J., 2015. Mooring system diagnosis and structural reliability control for position moored vessels. Control Eng. Pract. 36 (0), 12–26.

Fang, S., Leira, B., Blanke, M., 2011. Reliability-based dynamic positioning of floating vessels with riser and mooring system marine 2011. In: MARINE 2011—Computational Methods in Marine Engineering IV, pp. 113–121.

Fossen, T., Perez, T., 2009. Kalman filtering for positioning and heading control of ships and offshore rigs. IEEE Control Syst. Mag. 29 (6), 32–46.

Fossen, T.I., 2000. Nonlinear passive control and observer design for ships. Model. Identif. Control 21 (3), 129–184.

Fossen, T.I., 2011. Handbook of Marine Craft Hydrodynamics and Motion Control. John Wiley and Sons, Ltd, Chichester, UK, April.

Fossen, T.I., Perez, T., 2010. Marine Systems Simulator (MSS). ⟨http://www.marinecontrol.org⟩.

Fu, M., Ding, F., Li, M., Yi, P., 2010. A nonlinear estimate filter designed for ship dynamic positioning. In: The Eighth IEEE International Conference on Control and Automation, pp. 914–919, June.

Fu, M., Ning, J., Wei, Y., 2011. Fault-tolerant control of dynamic positioning vessel by means of a virtual thruster. In: 2011 International Conference on Mechatronics and Automation (ICMA), pp. 1706–1710, August.

Furuta, K., 1990. Sliding mode control of a discrete system. Syst. Control Lett. 14 (2), 145–152.

Hirdaris, S., Bai, W., Dessi, D., Ergin, A., Gu, X., Hermundstad, O., Huijsmans, R., Iijima, K., Nielsen, U., Parunov, J., Fonseca, N., Papanikolaou, A., Argyriadis, K., Incecik, A., 2014. Loads for use in the design of ships and offshore structures. Ocean Eng. 78, 131–174.

IMCA, 1994. Dynamic Positioning Station Keeping Incidents—Incidents reported for 2007. Technical Report, International Maritime Organization.

Isherwood, R., 1972. Wind resistance of merchant ships. Trans. Inst. Naval Arch. 115, 327–338.

Jetto, L., Longhi, S., Venturini, G., 1999. Development and experimental validation of an adaptive extended Kalman filter for the localization of mobile robots. IEEE Trans. Robot. Autom. 15, 219–229.

Johansen, T., Bo, T., Mathiesen, E., Veksler, A., Sørensen, A., 2014. Dynamic positioning system as dynamic energy storage on diesel-electric ships. IEEE Trans. Power Syst. 29 (November (6)), 3086–3091.

Khandekar, A., Malwatkar, G., Patre, B., 2013. Discrete sliding mode control for robust tracking of higher order delay time systems with experimental application. ISA Trans. 52 (1), 36–44.

Lorentzen, T., Blanke, M., 2005. SaTool Software Reference. Technical Report, DTU Elektro.

Loria, A., Fossen, T., Panteley, E., 2000. A separation principle for dynamic positioning of ships: theoretical and experimental results. IEEE Trans. Control Syst. Technol. 8 (March (2)), 332–343.

Luenberger, D.G., 1971. An introduction to observers. IEEE Trans. Autom. Control 16 (6), 596–602.

Mora, M.C., Tornero, J., 2008. Path planning and trajectory generation using multi-rate predictive artificial potential fields. In: IEEE/RSJ International Conference on Intelligent Robots and Systems, pp. 2990–2995.

Morishita, H., Souza, C., 2014. Modified observer backstepping controller for a dynamic positioning system. Control Eng. Pract. 33, 105–114.

MSC/IMCA, 1994. Guidelines for Vessels with Dynamic Positioning Systems. Technical Report, Internation Maritime Organization.

Muhammad, S., Dòria-Cerezo, A., 2012. Passivity-based control applied to the dynamic positioning of ships. IET Control Theory Appl. 6 (March (5)), 680–688.

Nguyen, D., Sørensen, A., 2009. Setpoint chasing for thruster-assisted position mooring. IEEE J. Ocean. Eng. 34 (October (4)), 548–558.

Perera, L., Oliveira, P., Guedes Soares, C., 2012. Maritime traffic monitoring based on vessel detection, tracking, state estimation, and trajectory prediction. IEEE Trans. Intell. Transp. Syst. 13 (September (3)), 1188–1200.

Perez, T., Fossen, T. I., Sørensen, A.J., 2004. A Discussion About Seakeeping and Manoeuvring Models for Surface Vessels. Mss-tr-001, Centre for Ships and Ocean Structures (CESOS), Norwegian University of Science and Technology NTNU, Trondheim, Norway. ⟨http://www.cesos.ntnu.no/mss⟩.

Phillips, D., 1996. The dynamic positioning of ships: the problems solved? In: UKACC International Conference on Control, vol. 2, pp. 1214–1219.

Phillips, D.F., 1998. Classic single-point failures of redundant DP systems. In: Proceedings of the Dynamic Positioning Conference, Houston, USA, pp. 1–8, October.

Skjetne, R., Smogeli, Ø.N., Fossen, T.I., 2004. A nonlinear ship manoeuvering model: identification and adaptive control with experiments for a model ship. Model. Identif. Control 25 (1), 3–27.

Sørensen, A., Sagatun, S., Fossen, T., 1996. Design of a dynamic positioning system using model-based control. Control Eng. Pract. 4 (March (3)), 359–368.

Sørensen, A.J., 2011. A survey of dynamic positioning control systems. Annu. Rev. Control 35 (1), 123–136.

Strand, J., Fossen, T.I., 1999. Nonlinear passive observer design for ships with adaptive wave filtering. New Directions in Nonlinear Observer Design, vol. 244. Springer, Berlin, Heidelberg, pp. 113–134.

Tannuri, E.A., Agostinho, A.C., 2010. Higher order sliding mode control applied to dynamic positioning systems. In: Proceedings of the Eighth IFAC Conference on Control Applications in Marine System, Rostock-Warnemunde, Germany, pp. 132–137, September.

Utkin, V., 1992. Sliding Modes in Control and Optimization. Springer-Verlag, Berlin, Germany.

Wang, S., Dinavahi, V., Xiao, J., 2013. Multi-rate real-time model-based parameter estimation and state identification for induction motors. IET Electr. Power Appl. 7 (January (1)), 77–86.

Wang, Y., Nguyen, B.M., Fujimoto, H., Hori, Y., 2014. Multirate estimation and control of body slip angle for electric vehicles based on onboard vision system. IEEE Trans. Ind. Electron. 61 (February (2)), 1133–1143.

Xia, G., Shi, X., Fu, M., Wang, H., Bian, X., 2005. Design of dynamic positioning systems using hybrid CMAC-based PID controller for a ship. In: 2005 IEEE International Conference Mechatronics and Automation, vol. 2, pp. 825–830.